Available online at www.sciencedirect.com

ScienceDirect

Geochimica et Cosmochimica Acta 140 (2014) 1–19

Geochimica et Cosmochimica Acta

www.elsevier.com/locate/gca

Process dominance shift in solute chemistry as revealed by long-term high-frequency water chemistry observations of groundwater flowing through weathered argillite underlying a steep forested hillslope

Hyojin Kim [a,*], James K.B. Bishop [a,b], William E. Dietrich [a], Inez Y. Fung [a]

[a] Department of Earth and Planetary Science, University of California, Berkeley, McCone Hall 307, Berkeley, CA 94720, USA
[b] Lawrence Berkeley National Laboratory, 1 Cyclotron Rd., Berkeley, CA 94720, USA

Received 12 November 2013; accepted in revised form 10 May 2014; available online 23 May 2014

Abstract

Significant solute flux from the weathered bedrock zone – which underlies soils and saprolite – has been suggested by many studies. However, controlling processes for the hydrochemistry dynamics in this zone are poorly understood. This work reports the first results from a four-year (2009–2012) high-frequency (1–3 day) monitoring of major solutes (Ca, Mg, Na, K and Si) in the perched, dynamic groundwater in a 4000 m^2 zero-order basin located at the Angelo Coast Range Reserve, Northern California. Groundwater samples were autonomously collected at three wells (downslope, mid-slope, and upslope) aligned with the axis of the drainage. Rain and throughfall samples, profiles of well headspace pCO_2, vertical profiles and time series of groundwater temperature, and contemporaneous data from an extensive hydrologic and climate sensor network provided the framework for data analysis.

All runoff at this soil-mantled site occurs by vertical unsaturated flow through a 5–25 m thick weathered argillite and then by lateral flows to the adjacent channel as groundwater perched over fresher bedrock. Driven by strongly seasonal rainfall, over each of the four years of observations, the hydrochemistry of the groundwater at each well repeats an annual cycle, which can be explained by two end-member processes. The first end-member process, which dominates during the winter high-flow season in mid- and upslope areas, is CO_2 enhanced cation exchange reaction in the vadose zone in the more shallow conductive weathered bedrock. This process rapidly increases the cation concentrations of the infiltrated rainwater, which is responsible for the lowest cation concentration of groundwater. The second-end member process occurs in the deeper perched groundwater and either dominates year-round (at the downslope well) or becomes progressively dominant during low flow season at the two upper slope wells. This process is the equilibrium reaction with minerals such as calcite and clay minerals, but not with primary minerals, suggesting the critical role of the residence time of the water. Collectively, our measurements reveal that the hydrochemistry dynamics of the groundwater in the weathered bedrock zone is governed by two end-member processes whose dominance varies with critical zone structure, the relative importance of vadose versus groundwater zone processes, and thus with the seasonal variation of the chemistry of recharge and runoff.

1. INTRODUCTION

On landscapes underlain by soil-mantled bedrock, many studies have suggested that significant runoff to channels occurs through the weathered bedrock zone beneath the soil

* Corresponding author. Tel.: +1 510 277 5616.
E-mail address: hyojin820@berkeley.edu (H. Kim).

http://dx.doi.org/10.1016/j.gca.2014.05.011
0016-7037/

(e.g. Wilson and Dietrich, 1987; Montgomery et al., 1997; Uchida et al., 2003; Haria and Shand, 2004; Tromp-van Meerveld et al., 2007; Calmels et al., 2011; Salve et al., 2012). This runoff drives weathering in this "critical zone" (e.g. Anderson et al., 2007), but theory and observations are limited regarding controls on the chemical evolution of these waters. Field studies that have included the weathered bedrock have demonstrated that rainwater infiltrates into the underlying bedrock and is perched at a depth where hydraulic conductivity is strongly reduced-perhaps associated with the transition to the largely unaltered bedrock-then travels downslope (e.g. Wilson and Dietrich, 1987; Montgomery et al., 1997; Uchida et al., 2003; Haria and Shand, 2004; Tromp-van Meerveld et al., 2007; Salve et al., 2012). To recharge groundwater through the weathered bedrock zone, water has been hypothesized to move preferentially through fractures (e.g. Mulholland et al., 1990; Montgomery et al., 1997; Banks et al., 2009; Salve et al., 2012). Because of localized permeability reduction, the bedrock flow may exfiltrate back into the overlying soil (e.g. Wilson and Dietrich, 1987; Montgomery et al., 1997), mixing with the soil water and rainwater. The chemical evolution of bedrock flows for a given lithology are thought to be determined by reaction times (e.g. Anderson et al., 1997a,b; Anderson and Dietrich, 2001; Asano et al., 2003), flow path (e.g. Shand et al., 2005; Shand et al., 2007) and interaction with matrix water (e.g. Legout et al., 2007; Jin et al., 2011).

Stream and spring chemistry have been used to conceptualize the residence times and flow-paths of subsurface flows of hillslopes (e.g. Rice and Bricker, 1995; Campbell et al., 1995; Holloway and Dahlgren, 2001; Calmels et al., 2011). During high-flow regimes, such as rain or snowmelt seasons, relatively shallow groundwater may flow rapidly through the hillslope (e.g. Anderson et al., 1997b). Thus, fast reactions on time scales of hours to days-ion exchange reactions and dissolution/precipitation of poorly crystalline secondary minerals—are thought to dictate the shallow groundwater's chemistry (e.g. Anderson et al., 1997a; Mulholland et al., 1990; Williams et al., 1993; Campbell et al., 1995). During low-flow regimes, as the water table progressively recedes, groundwater is thought to gain solutes via more extensive chemical weathering of the bedrock (e.g. Mulholland et al., 1990; Rice and Bricker, 1995; Campbell et al., 1995; Holloway and Dahlgren, 2001). Calmels et al. (2011), analyzing the chemistry of Liwu River in Taiwan, deduced that deep groundwater might contribute a significant fraction of river solute fluxes. As noted above, these hypotheses are primarily based on stream chemistry observations. Although stream chemistry observations are useful for quantifying chemical weathering fluxes, little is known about water residence times, flow-paths, and chemical weathering processes occurring inside the hillslope, all of which are fundamental to the understanding of chemical weathering processes and contaminant transport.

To reveal the processes that govern chemical weathering and solute fluxes in the weathered bedrock zone, direct observations of groundwater dynamics at high temporal and spatial resolution over annual hydrological cycles (from recharging to discharging) are needed. While the spatial variability of groundwater chemistry has been studied at many sites (e.g. Kenoyer and Bowser, 1992; Appelo and Postma, 2005), its temporal variability has received little attention. Previous studies have inferred groundwater chemistry in the weathered bedrock either by mass balance calculations based on soil water and stream (runoff) water chemistry (e.g. Anderson et al., 1997b; Holloway and Dahlgren, 2001; Anderson and Dietrich, 2001) or by direct sampling and analysis of water samples taken from springs/groundwater seeps in the riparian zone (e.g. Rice and Bricker, 1995; Soulsby et al., 1998; Anderson and Dietrich, 2001; Asano et al., 2003; Calmels et al., 2011) or from wells (e.g. Mulholland et al., 1990; Soulsby et al., 1998; Jin et al., 2011). Soulsby et al. (1998) sampled wells weekly, but other studies employing wells have relied on less frequent sampling (i.e. monthly–episodic). A few studies directly sampled groundwater in the weathered bedrock zone but only did so episodically, and were unable to resolve temporal dynamics (e.g. Shand et al., 2005, 2007; Banks et al., 2009). The temporal variability of conservative tracers (i.e. Cl^-, $\delta^{18}O$) in the bedrock groundwater has been monitored at higher frequency (i.e. weekly–monthly) for up to two years (Van der Hoven et al., 2005; Legout et al., 2007; Rouxel et al., 2011). To our best knowledge, no study has observed the high-frequency temporal dynamics of reactive tracers (i.e. weathering products, Ca, Mg, Na, K, Si) in the weathered bedrock zone. Such observations are necessary to reveal processes that control development of the weathering zone as well as the seasonal dynamics of solute flux to channels.

Here, we report the first results from multi-year, high-frequency (1–3 days) observations of the chemistry of a groundwater system flowing through a thick weathered bedrock zone (5–25 m) underlying a soil-mantled steep forested hillslope located at Angelo Coast Range Reserve, Northern California. At this site, Salve et al. (2012) showed that the groundwater, which is perched on the fresh bedrock boundary and flows through the weathered bedrock zone, generates all runoff. This report focuses on the chemical dynamics of this perched groundwater. Stream water samples from the adjacent creek, Elder Creek, will be reported separately. We measured the temporal and spatial variability of major solutes in the groundwater, rainwater, and throughfall. We also monitored basic physical–chemical parameters (temperature, pH, conductivity, and dissolved oxygen) at higher frequency (15 min). A limited suite of solid samples has been analyzed for clay mineral composition and cation exchange capacity. The major objectives of this study are: (1) documentation of the multi-year high-frequency dynamics of the groundwater chemistry along the hillslope; and (2) identification of the primary chemical processes that dictate water chemistry dynamics.

2. METHODS

2.1. Site description

Our site, dubbed "Rivendell", is a steep, forested, north-facing hillslope (4000 m^2; average slope 32°) in Angelo

Coast Range Reserve (39°43′47″N, 123°38′34″W http://angelo.berkeley.edu), located along Elder Creek, a tributary of the South Fork of the Eel River in Northern California (Fig. 1a). The reserve is one of the University of California's Natural Reserves.

The site is underlain by the Coastal Belt of the Franciscan Complex (McLaughlin et al., 2000) and is mainly argillite, with near-vertical dip and a strike that runs perpendicular to slope (i.e. north–south). A localized sandstone outcrop is exposed along the eastern divide of Rivendell (Lock et al., 2006; Fig. 1a), and thin (centimeters) interbeds of sandstone can be found in some of the outcrops exposed along a road cut across the site. This study area rose above the sea level about 2 million years ago during the passage of the Mendocino triple junction. Current channel incision rate at Elder Creek is about 0.2 mm y^{-1} but may have been closer to 0.4 mm yr^{-1} in the late Pleistocene (Fuller et al., 2009). A thin soil layer (0.5–0.75 m) overlies thick weathered bedrock (5–25 m). Major clay minerals are illite, Fe-rich chlorite, kaolinite and mixed layer illite/montmorillonite. Major primary minerals are quartz K-feldspar, plagioclase and chlorite (see analysis methods and full results in Electronic Annex 1).

The climate of the site is a typical coastal Mediterranean regime – warm, dry summers and cold, wet winters. Mean annual precipitation at the meadow across the site during the study period was 1760 mm y^{-1} and rain was mostly concentrated during the winter (October–April). The average annual air temperature during this period was 10 °C, and the seasonal minimum and maximum temperatures were −8 and 32 °C, respectively. Temperatures in the deep weathered bedrock zone remain almost constant throughout the year (10–11 °C). Rivendell is covered with dense vegetation – up to 60 m tall Douglas-fir (*Pseudostuga menziesii*) trees form the upper canopy, and live oak (*Quercus wislizeni*), tan-bark oak (*Notholithocarpus densiflorus*), madrone (*Arbutus menziesii*), and California bay laurel (*Unbellularia California*) compose the lower canopy.

In September 2007, seven 5.1 cm-diameter wells (W1, W2, W3, W5, W6, W7 and W10; Fig. 1a) were drilled into fresh bedrock (Salve et al., 2012). The wells were lined with slotted (0.6 cm spacing) PVC (polyvinyl chloride) pipes. In August 2010, two 5.1 cm-diameter wells (W12, W13) and three 7.6 cm-diameter wells (W14, W15 and W16) were drilled (W16 is not shown in Fig. 1a because it is on the south side of the hillslope). These new wells were also lined with similarly slotted PVC pipes. Since 2007, the site has been intensively monitored at high-frequency (5–30 min) for water table levels, meteorology, tree sap-flow, soil moisture, and subsurface temperature (Fig. 1a). All installed instruments are powered by solar panels and data are recorded with seven Campbell Scientific Inc. data loggers. A radio link provides internet access and data are transmitted to the University of California, Berkeley (U.C. Berkeley) every 4 h.

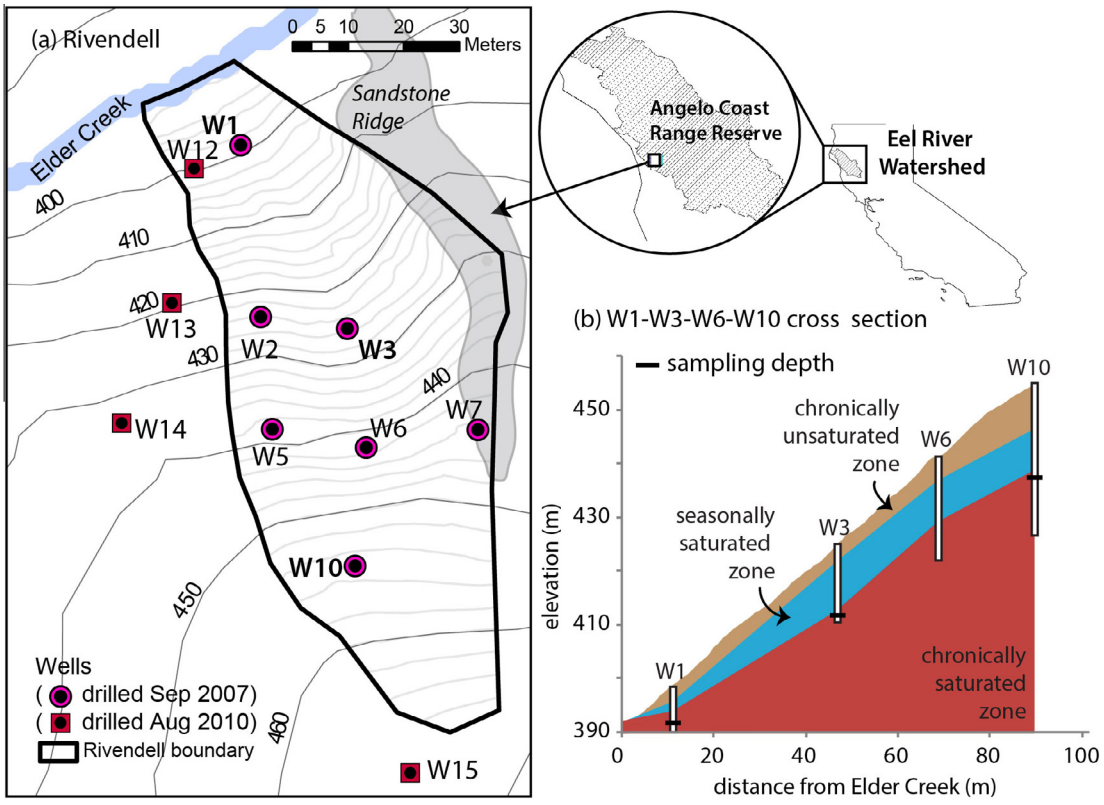

Fig. 1. (a) The study hillslope (Rivendell) is located at Angelo Coast Range Reserve, situated at the headwater of the Eel River Watershed, northern California. (b) Cross section of Rivendell (W1–W3–W6–W10) and the sampling depths of high-frequency sampling (solid black line).

2.2. High-frequency groundwater sampling

Three 24-position ISCO 6712 samplers (Teledyne ISCO, Lincoln, NE), modified with custom controllers for autonomous and remote operation (Kim et al., 2012), were used to sample the groundwater in three wells (Fig. 1a): W1 (since October 2008); W3 (since November 2009; and W10 (since March 2009). W1, W3, and W10 were drilled to 9.5 m, 14.4 m, and 27.4 m below the ground surface, respectively. The water table seasonally fluctuated between −4.5 and −2.3 m (W1), −10.7 and −2.8 m (W3), and −18.4 and −10.7 m (W10) (minus sign indicates distance below the surface). Water samples were collected from −6.7 m (W1), −11.7 m (W3), and −18.9 m (W10; Fig. 1b) depths that were within the chronically saturated zone. The sampling frequency was typically 1–2 days during the wet season and 1–3 days during the dry season. Each well water collection was 0.5–1 L, including purging and samples for analysis. Gaps in the time-series were due to power outages (winter time; mainly at W1 and W3) and unexplained failure of submersible pumps (Whale WP6012, Global Water Inc., Gold River, CA) installed in W3 and W10; the pumps were required to raise water to the ISCO at the surface when the water table was deeper than 8 m.

2.3. Sample preservation in the field

The ISCO samples were retrieved from the field site when all sample bottles were filled, resulting in a storage time of 3–4 weeks during the wet season and 1–2 months during the dry season. On every deployment day, we collected reference water samples at each well which were immediately processed following a standard water sampling protocol for trace metals (i.e. immediate filtration using 0.45 μm filters and acidification; US EPA 1996). We also measured pH and temperature of the reference samples (Accumet AP110 Portable pH Meter, Fisher Scientific, calibrated with standard buffers (pH 4 and 7)).

Early in the project, we used ISCO ProPak®LDPE 1000-mL sample bags that were open to the atmosphere. Compared to the reference samples, Na, K, Mg, and Si data were in complete agreement confirming that evaporation of ISCO samples was not detectable even during the summer dry season; however, we found that Ca in the bag samples from W1 and W3 were low in by as much as 30% as a result of $CaCO_3$ precipitation. In September 2009, we began developing an alternative sampling method to preserve the sample integrity not only for Ca but also for the redox sensitive elements, particularly Fe and Mn (Kim et al., 2012). Early prototypes deployed in late 2009 solved the Ca precipitation problem, and beginning October 2011, our new gravitational filtration system (GFS), which filters water through 0.45 μm pore-size Supor membranes within 30 min after the collection, achieved complete agreement with the reference samples for all elements (Kim et al., 2012). For Ca in W1 and W3, we thus report the early prototype, the GFS samples, and the reference samples. Data from W10, where we did not observe $CaCO_3$ precipitation, are reported for the entire time series.

2.4. Field measurements

Subsurface pCO_2 in the head-space of the wells was profiled at 1 m intervals using a pumped 0–30% SenseAir sensor K33-ICB (CO_2 Meters.com) from November 2011 through December 2012 during monthly (at times weekly) visits. The sensor was calibrated in the field using 2000 ppm and 5% dry gas standards. Achieved accuracy of 0.2% and 5% gas standards was 0.02% and 0.1%, respectively, after a temperature compensating correction.

A multi-parameter (YSI-600XL) probe was used to measure the vertical profiles of pH, temperature, conductivity, and dissolved oxygen (DO) in the water column at W3 and at W6 during the field visits. We used 1L of deionized (DI)–water that had been bubbled for 1 h using an aquarium pump to set 100% saturation DO; the pH probe was calibrated using pH 4 and 7 buffer solutions. We monitored temperature, pH, conductivity and DO at W6 at 15 min frequency from Feb. 2011–May 2011.

2.5. Rainwater and throughfall sampling

Bulk rainwater was collected from an open meadow across site, and throughfall–rain that passed tree canopy – was collected in the middle of the hillslope (at W7, Fig. 1b). The rainwater and throughfall collectors consisted of a PVC funnel connected to a polypropylene bottle. A #60 mesh screen in the neck of the PVC funnel was used to exclude >0.35 mm-sized solids from the sample. These samples were retrieved during and after every storm and stored in acid cleaned scintillation vials (20 mL) then periodically returned to Lawrence Berkeley National Laboratory (LBNL) for analysis.

2.6. Geochemistry characterization

Core samples from the drilling of wells were selected from W1, W3 and W10 holes to represent the three hydrologic subzones – unsaturated, seasonally saturated, and chronically saturated zones – and the soil samples were analyzed for (1) calcite content; (2) cation exchange capacity (CEC); and (3) DI-dissolvable salts (Table 1). The main purpose of these analyses was to characterize the chemical properties that are required to interpret the groundwater chemistry dynamics. All samples were air dried at the time of collection. 5–10 g of the core samples were crushed completely using a mortar and pestle and sieved using a 100-mesh (150 μm) sieve. Soil samples were collected from the first 10–15 cm from the ground surface, using a trowel in October and November 2011 during the field visits. The soil samples were air-dried and sieved using with the same mesh.

To determine calcite content, about 0.2 g of sample was added to 10 mL of 25% acetic acid and reacted overnight (Jin et al., 2010). The samples were occasionally shaken. These samples were centrifuged at 10,000 rpm for 30 min and the supernatant was decanted for the analysis. The calcite content was calculated by Eq. (1):

Table 1
Summary of the soil and bedrock geochemistry characteristics.

Location	Depth (m)		Calcite (wt.%)	DI-water ext. Si (mmole/kg)	CEC (meq/kg of soil or core)				
					Total	Ca_{ex}	Mg_{ex}	Na_{ex}	K_{ex}
W1	<0.01	Soil	1.73	1.54	608.50	508.47	74.19	1.94	23.89
	0.1		0.75	2.05	157.86	105.75	43.49	1.40	7.22
	0.5		0.70	3.06	154.33	92.70	51.86	3.03	6.74
	0.9	USZ[a]	1.04	2.51	157.86	124.66	24.07	2.52	6.62
	1.1		–	2.97	163.63	98.74	56.95	1.71	6.23
	3.6	SSZ[b]	1.10	2.31	183.49	124.87	49.88	2.39	6.34
	6.5	CSZ[c]	1.17	–	141.53	123.70	10.86	2.04	4.94
W3	<0.01	Soil	1.19	1.70	270.17	216.10	43.33	1.97	8.78
	1	USZ	0.73	1.56	176.85	122.55	48.88	1.84	3.59
	2.6		0.88	3.04	189.61	157.83	21.40	2.37	8.01
	4.1	SSZ	1.26	3.40	175.93	129.71	28.73	6.23	11.25
	9.3		3.62	1.82	333.10	224.38	100.00	3.27	5.45
	14.5	CSZ	3.30	1.84	259.81	159.43	86.41	2.73	11.23
W10	<0.01	Soil	0.61	1.05	142.92	107.93	22.43	1.68	10.89
	8	USZ	0.41	4.20	186.05	72.70	102.03	3.18	8.14
	10.8		0.99	4.16	227.15	118.70	94.36	3.60	10.49
	13.7	SSZ	1.00	2.11	204.41	109.12	86.59	3.15	5.55
	15.4		0.87	4.00	228.53	118.45	102.37	2.81	4.91
	16.7		0.86	3.39	171.72	103.28	55.28	3.05	10.11
	18.5		1.21	2.11	149.97	113.83	23.40	2.63	10.11
	24.4	CSZ	5.19	1.72	158.01	139.64	10.87	2.03	5.47

[a] Unsaturated zone.
[b] Seasonally saturated zone.
[c] Chronically saturated zone.

$$\text{calcite content}(\%) = \frac{\text{Ca(mole/L)} \times 0.01\text{L} \times 100.9\text{g/mole}}{0.2\text{g}} \times 100 \quad (1)$$

Cation exchange capacity (CEC) was determined using 0.2 g of the samples in 10 mL of a 0.1 M $BaCl_2$ −0.1 M NH_4Cl solution. The CEC samples were shaken at 180 rpm at 25 °C for 15 min and centrifuged at 2500 rpm for 20 min (Amacher et al., 1990) and the supernatant was decanted for the analysis. The CEC was estimated as the sum of the ionic concentrations of the extracted major cations (Ca, Na, Mg and K). To quantify easily dissolvable salt and silica phases, 0.5 g of the samples were added into 10 mL of DI water and reacted overnight at room temperature. The samples were occasionally shaken. These samples were centrifuged at 10,000 rpm for 30 min and the supernatants were decanted for the analysis. Of all the decanted solutions, visibly turbid ones were filtered using 0.45 μm Supor filters and others were not filtered.

2.7. Water sample handling and chemical analysis

All collected water samples were returned to LBNL for analysis. For major cations and Si analysis, the unfiltered ProPak water samples were filtered using 0.45 μm-Supor. The filtrates were then transferred to scintillation vials (20 mL) and acidified using Optima HNO_3. The early prototype GFS, and GFS samples were acidified using Optima HNO_3 to recover the precipitated Ca and trace metals, held for 24 h at room temperature, and then transferred to the scintillation vials. The rainwater and throughfall samples were acidified first to recover the adsorbed/coagulated trace metal phases and then filtered using 0.45 μm-Supor filters.

The samples of groundwater, rainwater, and throughfall were analyzed for major, minor, and trace elements using a Finnegan Element II magnetic sector inductively coupled plasma – mass spectrometer (ICP-MS) at LBNL. This study reports only five solutes – Ca, Mg, Na, K and Si. We included Si in ICP-MS analysis beginning in May 2011.

Instrument problems caused delays in analysis, such that the groundwater samples and the precipitation samples were analyzed within, on average, 1.3 years and 1.4 years after collection, respectively. We repeatedly analyzed selected set of the samples to evaluate the effect of evaporation during the storage. A few samples that were found to be at <10 mL of the expected 20 mL capacity of the scintillation vials and became concentrated by up to 60%, but most samples were insignificantly affected (10% variation) over 2 years. We excluded highly evaporated samples in this study.

The samples were run diluted and spiked with indium (In) as an internal standard. To validate the accuracy and precision of the ICP analysis, Certified River Water Reference Material for Trace Metals, SLRS-5 (National Research Council (NRC), Ottawa, ON, Canada) was analyzed in every run set. The % accuracy of these elements was calculated:

$$\%\ \text{accuracy} = \frac{C_A}{C_{SLRS}} \times 100 \quad (2)$$

where C_A and C_{SLRS} were the concentration of major cations identified by this study and NRC, respectively. In the case of Si, the reference value (65 μM) was obtained from Yeghicheyan et al. (2001). The percent accuracy ($n = 58$ runs) of Ca, Mg, Na, K and Si of this study were 99 ± 10 (standard deviation) %, 100 ± 10%, 97 ± 14% and 96 ± 13% and 105 ± 8%, respectively.

3. RESULTS

3.1. Geochemistry characteristics

Table 1 summarizes the results of the geochemistry characterization. The calcite content of the soil and bedrock samples were 0.61–1.73% and 0.41–5.19%, respectively. The CEC of the soil and bedrock was 143–608 meq kg^{-1} and 141–333 meq kg^{-1}, respectively, and Ca was the dominant exchangeable cation (50–90%), followed by Mg (10–50%; Table 1). Previous studies have pointed out that, for the calcareous soil samples, CEC, particularly extractable Ca, can be overestimated because of calcite dissolution. However, this effect is insignificant in acidic soils (Ciesielski and Sterckeman, 1997), and the magnitude of the effect correlates to the calcite content (Wang et al., 2005). The pH of Rivendell soils, determined by 1:1 = soil:DI water method (USDA, 2009), showed pH 4.8–6.2. In addition, Rivendell soil and bedrock contains relatively low calcite compared with the previous studies' values (e.g. 10–60%; Wang et al., 2005). Thus we conclude that although calcite might dissolve in the CEC analysis, its effect is negligible. The high CEC may be attributed to presence of illite/montmorillonite. The full results of the geochemistry analysis are in Electronic Annex 1.

3.2. Rainfall and throughfall inputs

Table 2 summarizes the volume weighted concentration of the solutes in the bulk rain and throughfall. The volume-weighted concentrations of Ca, Mg, Na and Si in bulk rainwater increased insignificantly after passing through the tree canopy: Ca (bulk rainwater (mM) vs. throughfall (mM); 0.003 vs. 0.01), Mg (0.005 vs. 0.008), Na (0.032 vs. 0.048), and Si (0.003 vs. 0.004), respectively. In contrast, the volume-weighted concentrations of K in throughfall (32 μM) were sixfold higher than in the bulk rainwater (5 μM).

3.3. Upslope (W10) and midslope (W3) areas

The concentrations of Ca, Na, K, Mg, and Si in W10 varied with water table level (Fig. 2 and Fig. 3), which shows a consistent annual cycle. Starting with the cessation of winter rain, the water table continuously receded, except for short duration responses (of 0.3–0.6 m) to the first significant rainstorms early in the following rainy season. Then, after a cumulative rainfall of 400–600 mm, the level rapidly rose from a depth of −18 m by 4 to 6 m within several days and remains high (rarely receding deeper than −14 m) for the rest of the rainy season, thus developing a water mass that we refer to as 'seasonal groundwater' (Fig. 2). As rain events continue, the water table rose sharply on each event and then recedes slowly. Relative to the dry season levels, the major cations in the seasonal groundwater were diluted by factors of ~18 (Ca; 2–0.11 mM), 3~5 (Mg; >0.35–0.1 mM), 2 (Na; 0.5–0.25 mM), and 5 (K; 50–9 μM), respectively, but Si increases from 0.3 to 0.4 mM (Fig. 3 and Table 2). During the early summer, as the water table depth falls below -16 m, the concentrations of major cations continuously increased while Si decreased (Fig. 3). W10's pH also varied with depth, ranging from ~6.7 to less than 5 at deepest and shallowest limits, respectively (Fig. 4). The pCO_2 in W10 varied from 2.5% to 5.9% at −5 m and from 3.7% to 7% at −10 m, respectively (Fig. 5).

Water chemistry and water table fluctuations at midslope W3 behaved similarly to that observed upslope at W10, but it differed in four ways. First, the water table at W3 was more dynamic in the winter (−9 to −4 m), responding to storms with a greater range than W10 (−14 to −12 m; Fig. 2). Second, the depth to the top of the seasonal groundwater fluctuating zone was shallower at W3 (~−3 m) compared with W10 (~−12 m). Third, W3 had a greater (4–6 m) and earlier response to the first rains compared with W10 (0.3–0.6 m). Fourth, during the rainy season, all cation concentrations at W3 varied significantly as the water table fluctuated in the seasonally saturated zone (Fig. 3).

During the summer recession, the major cation concentrations in W3 sharply increased as water level drops from −8 to −9 m (Fig. 3). The figure suggests that cation concentrations appeared to decrease as W3's water table continuously receded to deeper than −9 m, but this behavior is primarily an artifact of inter-annual concentration variability and incomplete time series sampling. The Si concentration response at W3 generally followed that seen at W10; Si increaseed from 0.2 to 0.4 mM as the water level rose from −10 to −5 m (Fig. 3), but decreased slightly at depths shallower than −4 m. At the shallowest water level, the Mg, K and Na concentrations in W3 were similar to those of W10 (Table 2). The lowest concentration of Ca in W3 was twofold higher than that in W10 (Table 2). The pH of W3 is ~5.6 and ~7.3 at shallow and deepest depths, respectively and was generally more basic than at W10 (Fig. 4). The pCO_2 of W3 sharply increased from the ground surface to 5–6% at -5 m and remained largely invariant at deeper depths (Fig. 5).

3.4. Downslope (W1) area

The behavior of the downslope well (W1) differed from that of both the mid-slope and upslope wells (Figs. 2 and 3). The water table depth closely followed the level of Elder Creek which serves as the lower boundary condition for the hillslope hydrology. Head gradient remains always towards the stream. During the winter, the water table was typically about −4 m and responds rapidly to rainstorms, with brief excursions reaching −2.3 m. However, the solute concentrations rarely changed from the typical dry season values (Figs. 2 and 3). The concentrations of Ca, Mg, Na, K, and Si in W1 remained around 1.71 mM, 0.31 mM, 0.41 mM, 26 μM, and 0.24 mM, respectively (Table 2).

Table 2
Summary of the solute concentration in bulk rainwater, throughfall, and Rivendell groundwater (W1, W3 and W10) during the high flow and low flow regime.

	Ca (mM)	Mg (mM)	Na (mM)	K (μM)	Si (mM)
Inputs					
Bulk rainwater	0.003	0.005	0.032	5	0.003
Throughfall	0.01	0.008	0.048	32	0.004
High flow regime (water table depth shallower than)					
W10 (>−13 m)	0.10	0.09	0.26	13	0.41
W3 (>−4 m)	0.24	0.10	0.23	10	0.30
W1 (dilute events only)	0.14	0.06	0.16	11	0.20
Low flow regime (water table depth deeper than)					
W10 (<−17.5 m)	1.14	0.36	0.36	30	0.30
W3 (<−8.5 m)	2.03	0.30	0.43	24	0.26
W1(<−4.1 m)	1.71	0.31	0.41	26	0.24

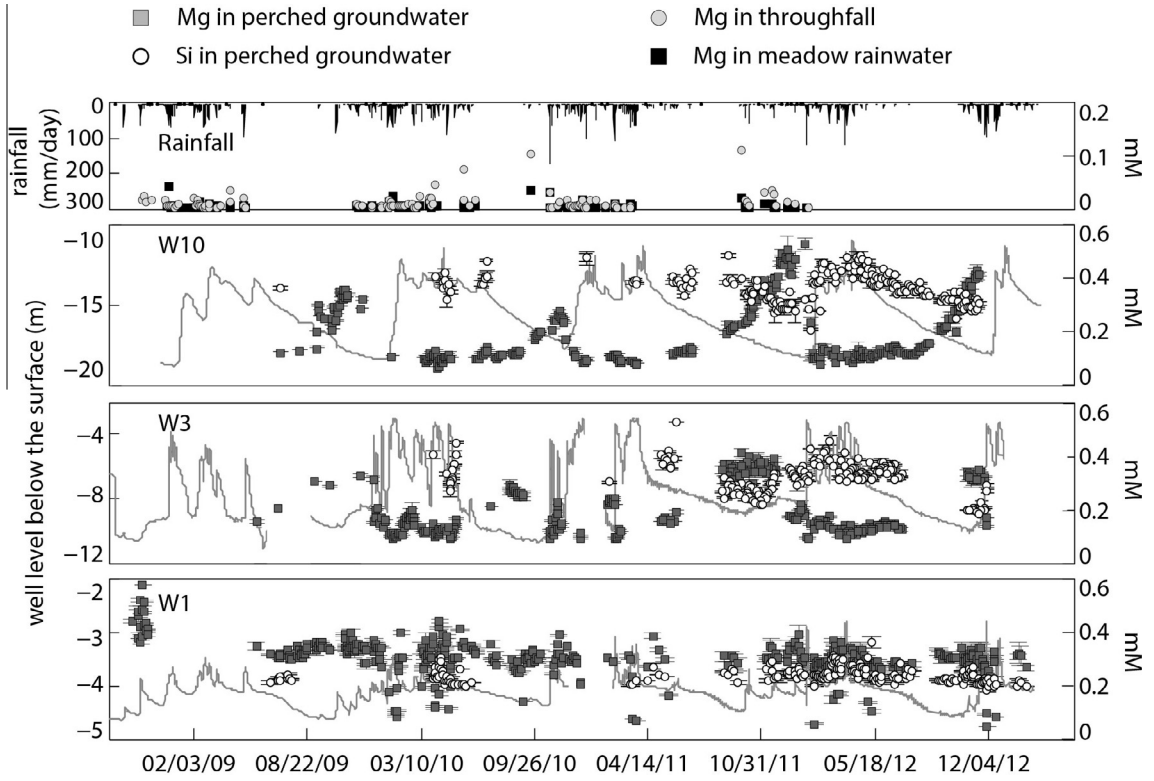

Fig. 2. (Top panel): Temporal variability of Mg in rainfall (closed square) and throughfall (gray circle) is shown on the top panel. (2nd–4th panels): Mg (gray squares) and Si (open circles) in the groundwater of Rivendell, observed at 1–3 days frequency with corresponding water table levels.

During some storms, the four major cations in W1 were significantly diluted as the water table rose, but recovered back to "pre-event" values within several days, synchronizing with the water table recession Figs. 2 and 3). The lowest concentrations of cations in W1 fell slightly lower than those of the upslope wells (Table 2). Remarkably, Si in W1 varied little from ~0.2 mM, even during the cation dilution events. The pH of W1 was invariant year round at pH 7 and briefly decreased to pH 6 during the dilution events. At W1, pCO_2 measured at -3 m varied from 0.7% to 2.7%.

4. DISCUSSION

4.1. Representativeness of the groundwater samples

Understanding of what these groundwater samples represent is crucial to further hydrochemical interpretation. Because of vertical hydraulic heads, and density and concentration gradients, the water column in a well tends to be mixed and reflects the chemical signature of the inflow from the surrounding aquifer (e.g. Gibs et al., 1993). At Rivendell, Salve et al. (2012) proposed that fracture density

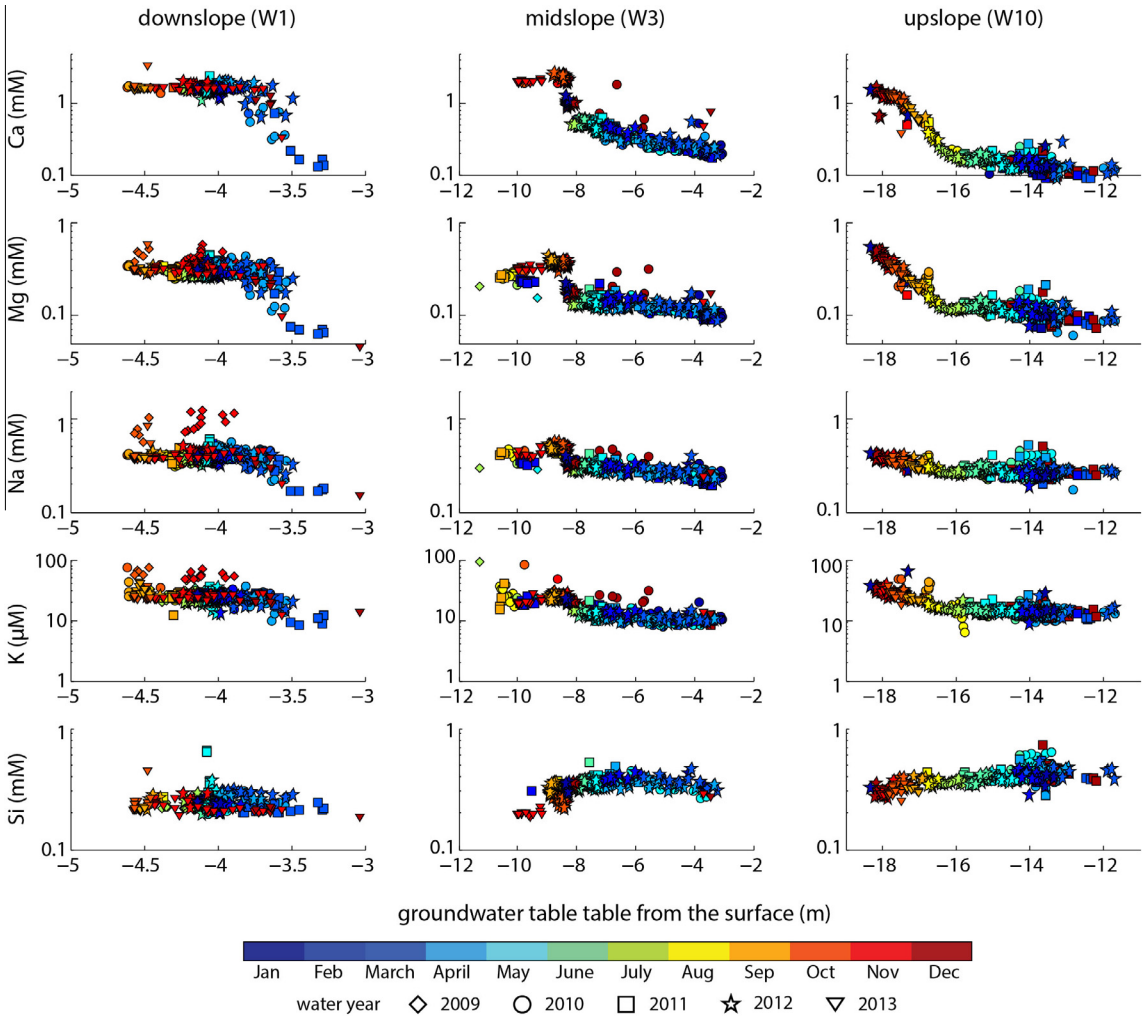

Fig. 3. Semi-log plots of the relationship between major cations and Si (1–3 days frequency) and well levels (daily average) for W1, W3 and W10 (water year 2009–2013). The solute concentrations (log scale) are plotted against well level below the surface (m). In case of Ca of W1 and W3, due to problems of $CaCO_3$ precipitation prior to 2009, only the new sampling design samples and reference samples were presented.

may decrease with depth; correspondingly, so would hydraulic conductivity. Hence, as the water table rises during the rainy winter, the water in the well is expected to become progressively more influenced by the shallower, more rapidly flowing water. Fig. 6 shows the water table recovery of the three wells after the ISCO sampling at various depths. W1 shows a rapid recovery, independent of season (Fig. 6a), whereas the recovery times at W3 (Fig. 6b–c) and W10 (Fig. 6d–e) become significantly longer with lowered water table. These variations suggest that the groundwater samples would be dominated by the flux-averaged flows from the seasonally saturated zone, despite the fact that the pump intake is located within the chronically saturated zone.

The water column in the Rivendell wells is expected to be completely mixed during the rainy season because the newly-arriving shallower groundwater is cooler than the pre-event groundwater. During the winter rain storms, the air temperature is cooler (mean precipitation-weighted air temperature = 7.7 °C for storms with total rainfall >10 mm; $n = 138$) than the groundwater (10.5–11.5 °C); thus, the infiltrated rainwater is likely denser than the pre-event groundwater. The temperature time-series measured during a series of storms from March 11 to April 1 2011 demonstrate this temperature behavior (Fig. 7). During this time, the temperature probe was at −11.6 m, about 5–7 m below the water surface. The water temperature at W6 decreased from 10.7 to 10.4 °C as the water table rose and the average air temperature during this series of storms was 4.4–5.7 °C (Fig. 7). These observations show that the new water was, at least, 0.3 °C colder or 0.04 kg m^{-3} denser than the pre-event groundwater, thus setting up convective mixing inside the well (Martin-Hayden, 2000).

During the summer a strong thermal stratification to a depth of several meters may develop and inhibit mixing (Fig. 8a), but the nearly constant temperature profiles during the late rainy season (Feb. 2011–May 2011) indicate rapid mixing inside the well (Fig. 8b). In addition, the average temperature of the entire water column at W6 shifts with season, again consistent with complete mixing

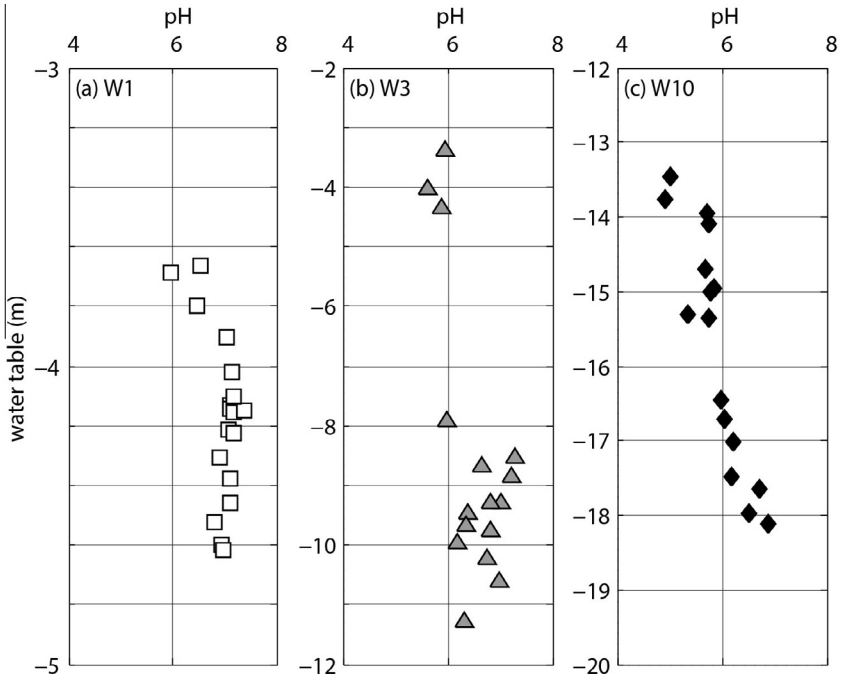

Fig. 4. The relationship between pH and water table depths at (a) W1, (b) W3 and (c) W10. The pH of the groundwater was measured during the monthly field visits from 2009 to 2011.

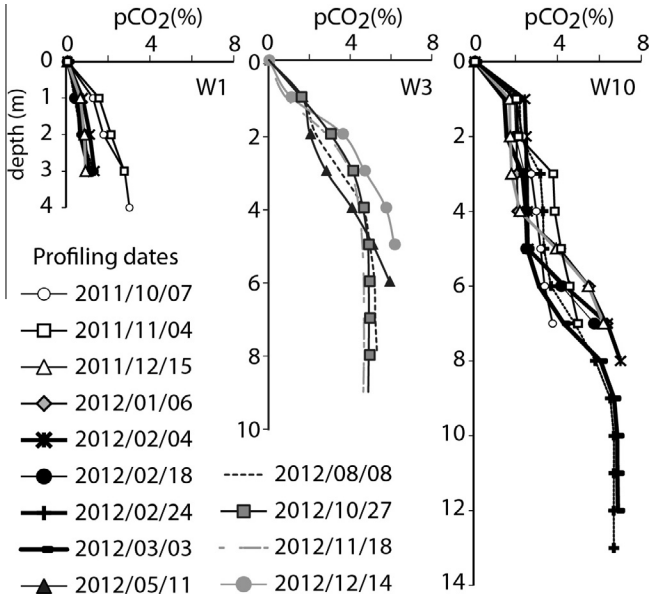

Fig. 5. Profiles of pCO_2 in well headspaces of W1, W3 and W10 from October 2011 to December 2012 at Rivendell.

(Fig. 8b). Altogether, the observations in Figs. 7 and 8 suggest that cool winter storms introduce recharging water that is generally cooler than the pre-existing well-water. Inside the wells, this initial thermal gradient leads to convective mixing, resulting in uniform temperature profiles. The ISCO sampling removes a relatively minor amount (20 cm) of water, and does not disrupt this mixing. The pump port, located at depths within the chronically saturated zone (Fig. 1b), collects this mixed water; therefore the samples represent the rapid shallower flows during the winter and the slower deeper flows in the summer.

4.2. Mechanisms for the chemical dynamics of the seasonal groundwater

Over four years of high-frequency observations, we have identified repeating patterns of hydrology and water chemistry in all three wells. Table 2 summarizes the

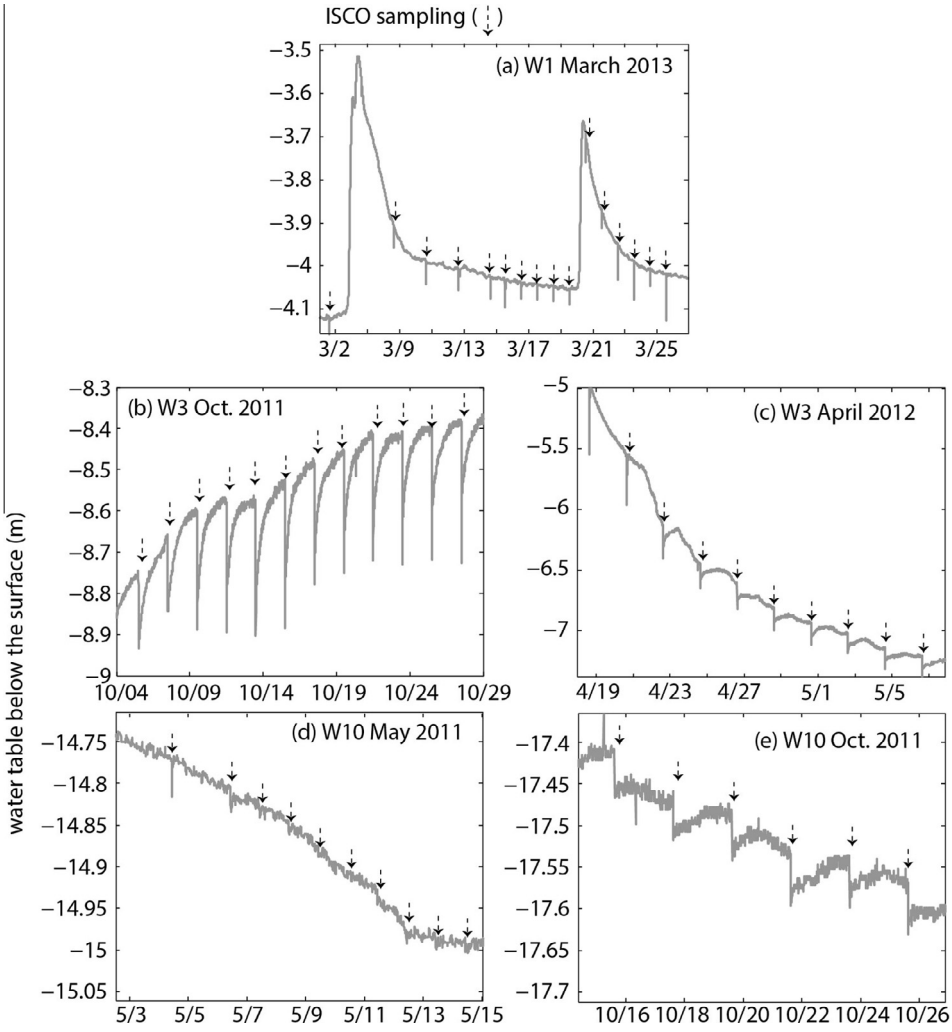

Fig. 6. Variation of water table responses to ISCO water sampling (1–3 day intervals), denoted by arrows, at (a) W1, (b–c) W3 and (d–e) W10.

concentrations of the five constituents in the rainfall, throughfall and groundwater. Because of the depth dependency of the concentrations, the depths of the water tables were used as criteria for the calculation. For W1, the minimum concentrations were averaged only for data of the dilution events. Rivendell receives insignificant inputs of Ca, Mg, Na and Si from rainfall and throughfall, but throughfall introduced a substantially high K into Rivendell (Table 2). Potassium is an essential nutrient and trees absorb (via roots) and release (via canopy and litter) a significant amount of this element (Sollins et al., 1980). However, in the deeper weathered-bedrock zone, where the impact of vegetation is less, K in the groundwater progressively increases, from the wet season to the dry season (at W3 and W10; Fig. 3).

We do not know the exact chemistry of the flow through the unsaturated zone that recharges the seasonal groundwater, but dilution of the solute concentration in the groundwater as the water table rises indicates that these waters are more dilute than the pre-event groundwater but more concentrated than the throughfall. This suggests that processes in the unsaturated zone play a significant role in determining the chemistry of the water arriving at the wells. We suggest that two end-member processes are controlling the groundwater's solute concentrations throughout the year:

1. When the water table is shallow at the upslope and mid-slope wells and is transiently seen at W1, concentrations are low and decrease as the water table rises. We suggest these concentrations arise as infiltrated rainwater gains cations by the cation exchange reactions enhanced by high subsurface pCO_2, and that increases in Si may be due to the dissolution of amorphous silica in the unsaturated zone.
2. When the water table is deep and dropping at mid-slope and upslope wells and is seen most of the time at W1 the concentrations increase towards high values. Here we suggest that this increased solute concentration is governed by thermodynamic equilibrium with specific minerals within the weathered argillite.

4.2.1. *Cations controlled by exchange reactions and pCO_2*

One of the most remarkable features of our high-frequency observations is the similarity of the solute concentrations for a given water table level throughout storms,

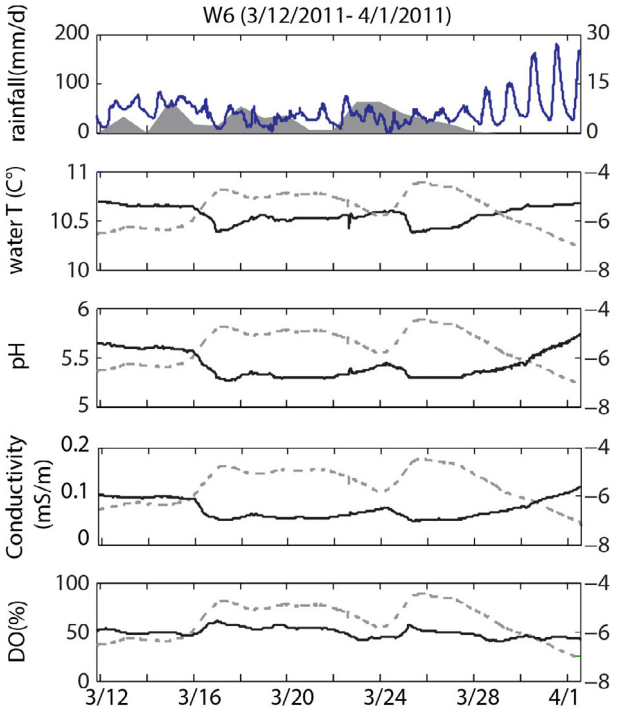

Fig. 7. High-frequency (15 min) time-series of water temperature, pH, conductivity, and DO (%) in W6 from March 12 2011–April 1 2011. The water level of W6 is also shown in dotted gray lines. The top panel shows air temperature (blue line) and rainfall (gray).

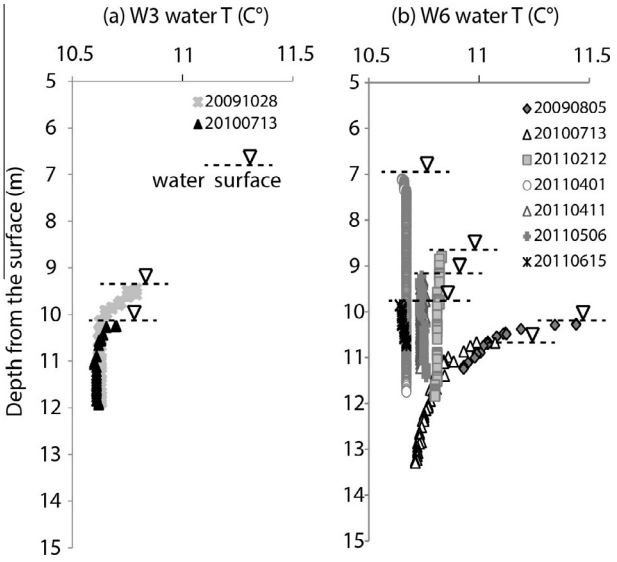

Fig. 8. Vertical profiles of the water temperature of (a) W3 and (b) W6. W3' profiles were measured in September 2009 and July 2010, and W6's profiles were measured seven times between 2009 and 2011 during the monthly site visits.

seasons and years for each well (Fig. 3 and Fig. 9). The water-temperature time-series (Fig. 7) suggests that the infiltrated rainwater is delivered to the water table before becoming thermally equilibrated with the soil and bedrock; thus chemical reactions that are fast enough to reach equilibrium concentrations on hour to day timescales are responsible for low concentrations at high winter flows.

Numerous studies have proposed cation exchange reactions as an essential process to determine soil and eventually stream chemistry, particularly for high flow regimes (e.g. Mulholland et al., 1990; Cerling et al., 1989; Williams et al., 1993; Anderson et al., 1997a; Cosby et al., 1985; Campbell et al., 1995; Jin et al., 2011). Cation exchange reactions involve the interaction between positively charged electrolytes in solution and weakly-bound cations on the soil/bedrock mineral surface. Oh and Richter Jr. (2004), via column leaching experiments, demonstrated that as CO_2 increased from 1% to 10%, the cation yield increased nearly twofold (34–69 meq kg^{-1}). They estimated that approximately 60–70% of the total cations were produced by the exchange of protons, with the remainder supplied by mineral dissolution. Our site has high CEC (141–608 meq/kg) and elevated-pCO_2, which suggests the critical role of CO_2 in the cation exchange reactions in determining the solute concentrations.

The equilibrated solute concentration with Rivendell's cation exchangers and pCO_2 were simulated using PHREEQC (Appelo and Postma, 2005; Table 3). We assumed that the cation exchange reactions reach equilibrium in the unsaturated zone. Inputs to the model were averaged exchangeable cations (Ex. in Table 3) available at each well. The subsurface pCO_2 of W1, W3 and W10 varied significantly with depth and time, we thus simulated reactions with the measured minimum, average, and maximum pCO_2 values at each well. The ion selectivity coefficients (K_{GT}) for the reactions were estimated using equations from Tournassat et al. (2009). We assumed binary-exchange reactions (Na–Ca, Na–Mg, and Na–K) for the ion selectivity coefficient. The input water was assigned the averages volume-weighted concentration of Ca, Mg, Na and K in the throughfall. The minimum pCO_2 (1%) predicted lower values than the measured for the winter low concentration case (Table 3). As pCO_2 was elevated, however, the predicted values showed a good agreement with the measured values. In some cases, the simulated Mg concentrations were lower (up to 40%) than the measured values even at the highest pCO_2, suggesting other mineral weathering reactions may play a role in compensating this difference.

Fine pores and dead-end fractures in soils and rocks may hold water for long times. We did not measure soil water chemistry; however, it is reasonable to assume that the less mobile soil and rock waters are highly concentrated in solutes. We propose that cations are chemically mobilized from the mineral structure continuously but remain locked in the less mobile soil and rock waters and weakly bound to the mineral surfaces. During the rainy season, these cations are transferred to the mobile water via the proton dominated cation exchange reactions.

4.2.2. Cations controlled by thermodynamic equilibrium

We hypothesize that high concentrations in the groundwater develops by further chemical alteration of the recharged water from the vadose zone. Fig. 10 shows that the groundwater was close to thermodynamic equilibrium

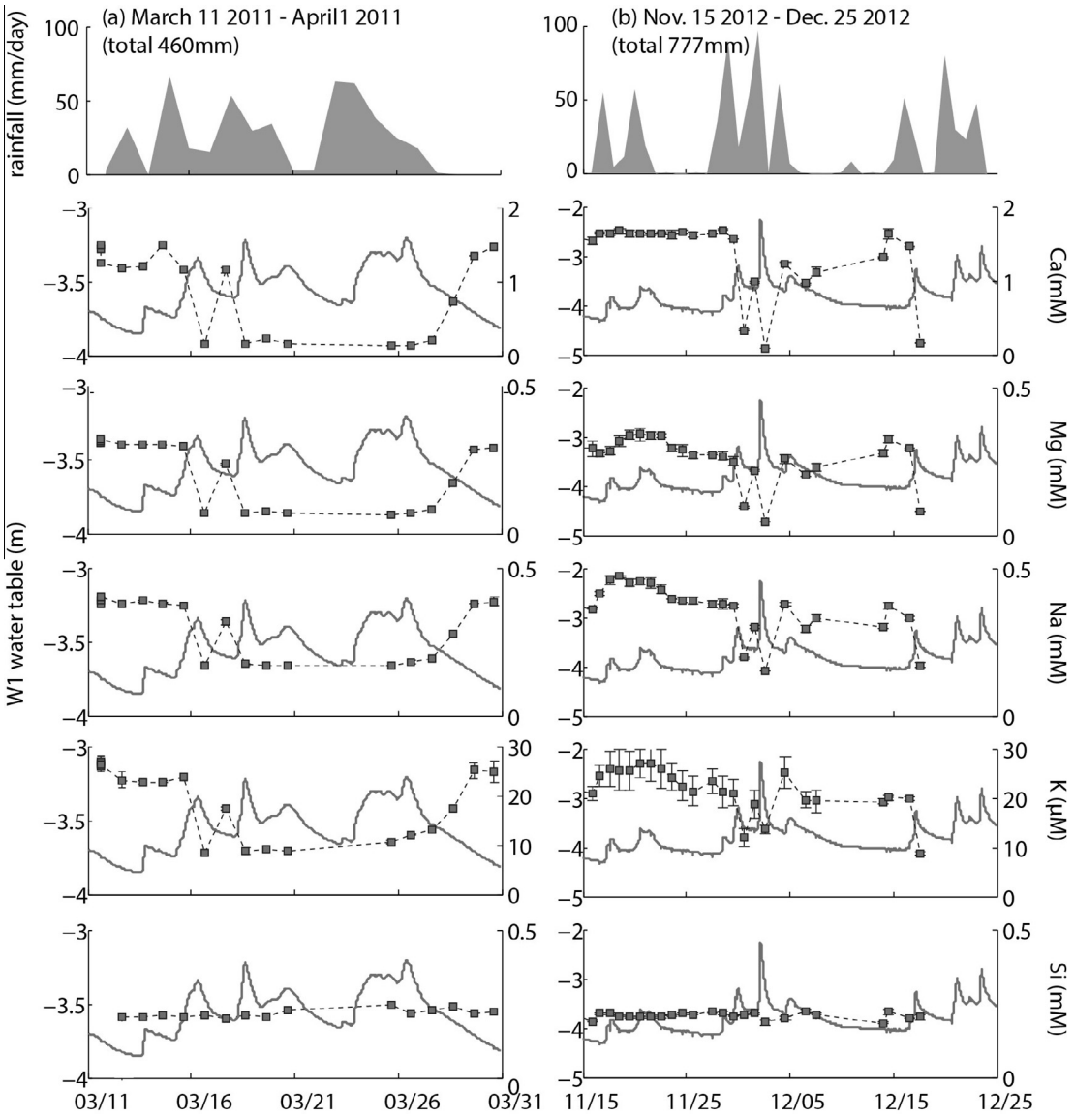

Fig. 9. Responses of major cations (Ca, Mg, Na, K) and Si in W1 during large rainstorms for two periods: March 11–April 1 2011 (left column), and Nov. 15-Dec. 2012 (right column). The light gray lines are the W1 water table.

with clay minerals, such as Fe- rich chlorite (Mg; Fig. 10a) and montomorillonite (K; Fig 10c), but were far from equilibrium with primary minerals, such as albite (Na; Fig 10b). We estimate the equilibrium reaction constants as follows:

Fe-rich chlorite (Kittrick, 1982):

$$(Si_{2.47}Al_{1.53})(Mg_{1.05}Fe_{3.29}Al_{1.60})O_{10}(OH)_8 + 18.07H^+ \Longleftrightarrow 1.05Mg^{2+}3.29Fe^{2+} + 3.13Al^{3+} + 2.47H_4SiO_4 + 8.10H_2O \quad pK_{sp} = 22.8 \pm 0.5$$

Montmorillonite-Kaolinite (Garrels, 1984):

$$K_{0.3}(Al_{1.9})(Si_4)O_{10}(OH)_2 + 0.1Al(OH)_3 + 0.7H_2O + 0.3H^+ \Longleftrightarrow Al_2Si_2O_5(OH)_4 + 2SiO_2 + 0.3K^+ \quad pK_{eq} = 5.80$$

Albite – Kaolinite (Faure, 1998):

$$2NaAlSi_3O_8 + 9H_2O + 2H^+ \Longleftrightarrow Al_2Si_2O_5(OH)_4 + 2Na^+ + 4H_4SiO_4 \quad pK_{eq} = -0.38$$

We assumed Al and Fe were equilibrated with gibbsite ($Al(OH)_3$, $pK_{sp} = 8.11$) and hematite (Fe_2O_3, $pK_{sp} = 0.9$) respectively, because these elements were shown to be mostly in colloidal forms in the Rivendell groundwater (Kim et al., 2012); hence, the measured values may overestimate their true concentrations in solution.

The equilibrium differences may be because of the various dissolution kinetics of source minerals. We did not measure the reactive mineral surface areas in Rivendell core samples. It is known that clay minerals generally have significantly higher surface area than primary minerals. For example, the surface area of montmorillonite (smectite), illite and chlorite are 600–800 m^2g^{-1}, 70–120 $m^2\,g^{-1}$ and 4–150 $m^2\,g^{-1}$, respectively (Essington, 2004; Jin et al., 2010). In contrast, that of K-feldspar and Na-feldspar are 0.03–2 and 0.003–4 $m^2\,g^{-1}$, respectively (White and Brantley, 2003).

Table 3
Simulated (PHREEQC) and measured cations in W1, W3 and W10 during the high flow regime.

Well 1 ($K_{GT}^{Na/Ca} = 0.56$[1]; $K_{GT}^{Na/Mg} = 0.63$[1]; $K_{GT}^{Na/K} = 1.23$[1])						
	Measured		PHREEQC			
Cations	Ex.[a]	W1[b]	pCO2 Input[b]	0.5% Output[b]	1.5% Output[b]	2.5% Output[b]
Ca	235	0.14	0.01	0.06	0.14	0.18
Mg	57	0.06	0.008	0.02	0.03	0.04
Na	2.12	0.16	0.05	0.13	0.18	0.21
K	12.62	0.01	0.03	0.05	0.07	0.09
Well 3 ($K_{GT}^{Na/Ca} = 0.56$[1]; $K_{GT}^{Na/Mg} = 0.66$[1]; $K_{GT}^{Na/K} = 1.23$[1])						
	Measured		PHREEQC			
Cations	Ex.[a]	W3[b]	pCO2 Input[b]	1% Output[b]	3% Output[b]	5% Output[b]
Ca	165	0.24	0.01	0.10	0.20	0.27
Mg	38	0.1	0.008	0.02	0.04	0.06
Na	2.06	0.23	0.05	0.20	0.27	0.31
K	6.79	0.01	0.03	0.05	0.07	0.08
Well 10 ($K_{GT}^{Na/Ca} = 0.69$[1]; $K_{GT}^{Na/Mg} = 0.63$[1]; $K_{GT}^{Na/K} = 1.23$[1])						
	Measured		PHREEQC			
Cations	Ex.[a]	W10[b]	pCO2 Input[b]	1% Output[b]	3% Output[b]	6% Output[b]
Ca	102	0.10	0.01	0.06	0.11	0.17
Mg	76	0.09	0.008	0.05	0.09	0.14
Na	2.90	0.26	0.05	0.2	0.27	0.34
K	8.77	0.01	0.03	0.06	0.08	0.10

[1] Estimated from Tournassat et al. (2009) using Eqs. (9) and (10).
[a] meq/kg of soil.
[b] mM.

Calcium concentrations in the higher concentration waters of W1 and W3 were at saturation with respect to calcite. At W1, except for the dilution events, pH was typically 7 (Fig. 4a) and the $pCO_2$was 1.5–2.5% near the water table (Fig. 5a). In this condition, calcite equilibrium yields 1.42–1.89 mM of Ca ($pK_1 = 6.46$, $pK_2 = 10.49$, $pK_H = 1.26$, $pK_{sp} = 8.41$ at 283 K; IAEA-UNESCO, 2001), in good agreement with the measured W1's Ca (1.71 mM; Table 2). At W3, during the late dry season when the water table was low, pH was approximately 6.8 (Fig. 4), $pCO_2$was 4–5%, (Fig. 5) and Ca concentration was 2.03 ± 0.4 (standard deviation) mM (Table 2). In this given condition, the calculated Ca concentration at calcite saturation is, 1.7–2.14 mM, which matches the measured Ca in W3. These thermodynamic calculations suggest that higher concentration waters are equilibrated with the relatively reactive minerals but not with the less reactive minerals, suggesting that limited residence time of the water in the fractured bedrock is an important factor determining the solute concentration.

4.2.3. Si concentrations

Silicon behaves in an opposite fashion compared to major cations; the maximum concentration of Si (Si_{max}) appears when the cations are in low concentration and the minimum (Si_{min}) appears at high concentrations of cations. Si_{max} is highest (0.5 mM) at W10 and decreases downslope to W1 (~0.25 mM). Si_{max} is likely regulated by rapid dissolution of aluminosilicates and/or amorphous silica (e.g. Kennedy, 1971; Clow and Drever, 1996; Asano et al., 2003). Kennedy (1971), based on the stream chemistry observations in Mattole River, Northern California, postulated that groundwater has lower Si than the water leached from soils. Rivendell soils may have a large pool of easily dissolvable Si as demonstrated via the DI-water extraction experiment (Table 1), suggesting dissolution of amorphous silica may determine Si_{max}. However, we note that, even though we assumed that all Si is in dissolved form, such as silicic acid, a significant fraction is possibly in colloidal form. The concentrations of Al and Fe in the groundwater strongly suggest a significant contribution of colloids, which may be associated with Si. To quantify the contribution of these two processes, a further study is required.

The high Si concentrations are supersaturated with respect to kaolinite, gibbsite, and quartz (Fig. 10d), but unsaturated with amorphous silica (2 mM; Sposito, 2008, 129p). Among the secondary minerals, gibbsite ($Al(OH)_3$), which is the most unstable, will precipitate first, but due to high Si concentration, may further transform to kaolinite.

$$2Al(OH)_3(s) + 2H_4SiO_4 \Longleftrightarrow Al_2Si_2O_5(OH)_4 + 5H_2O$$

If Si is controlled by kaolinite ($Al_2Si_2O_5(OH)_4$), then the equilibrium H_4SiO_4 concentration is between 0.005 (Essington, 2004; gibbsite-kaolinite (2) in Fig. 10d) and

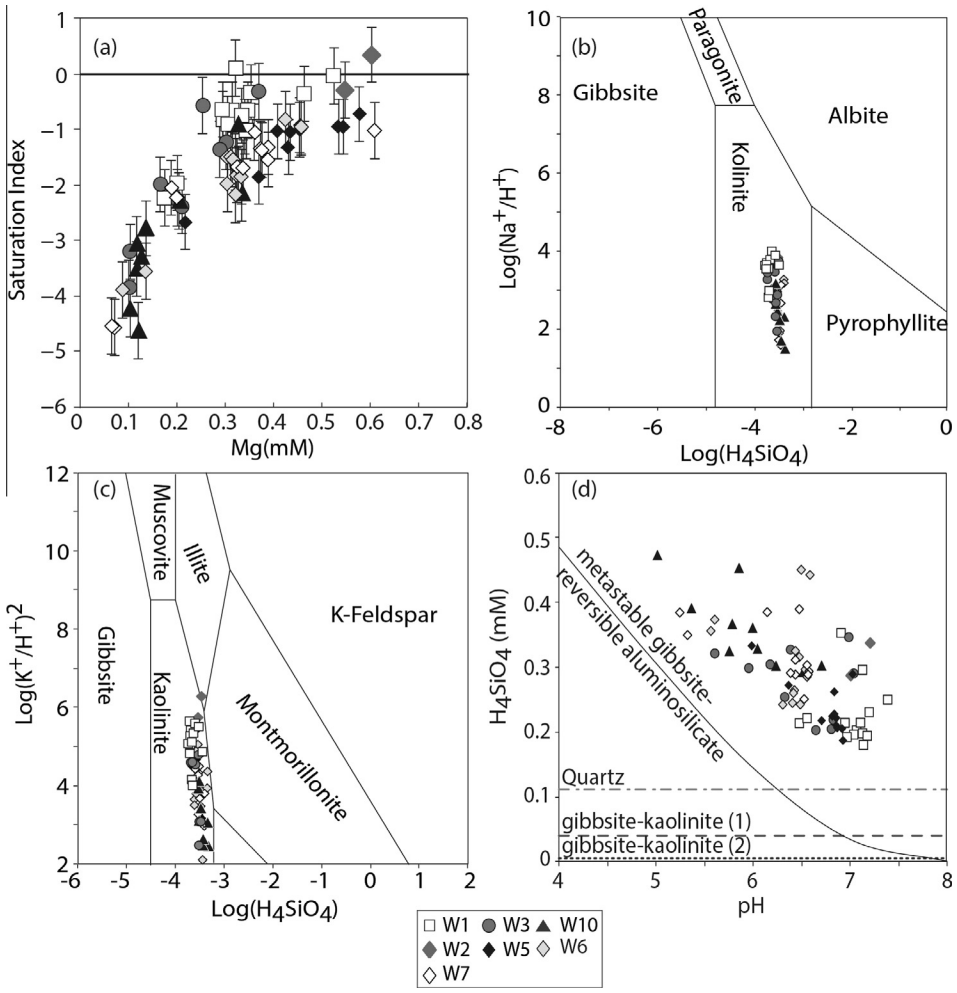

Fig. 10. (a) Saturation index of the Rivendell groundwater (reference samples) for the Fe-rich chlorite; (b) Stability diagram of albite (Na). The stability diagram is adapted from Faure (1998); (c) Stability diagram of feldspar-illite-montmorillonite. The stability diagram is adapted from Garrels (1984); (d) Equilibrium lines for aluminosilicate solids and secondary minerals which potentially control Si and Al in natural waters (i.e. gibbsite-reversible alumonsilicate, quartz, gibbsite-kaolinite) and the H_4SiO_4 concentrations and pH of Rivendell's reference samples. Equilibrium data are adapted from Essington (2004) for gibbsite-kaolinite (1) and quartz, Sposito (2008) for gibbsite-kaolinite (2), and Paces (1978) for gibbsite – reversible aluminosilicate, respectively. The close squares, gray circles and close triangles represent W1, W3, and W10, respectively. Diamonds in gray, black, light gray and open represent W2, W5, W6, and W7, respectively.

0.04 mM (Sposito, 2008; gibbsite-kaolinite (1) in Fig. 10d), regardless of pH. These values are, at least, fivefold lower than the observed Si_{min}, indicating that the high cation concentration water is supersaturated with respect to kaolinite.

Formation of well-crystalline kaolinite may be limited at ambient temperature and pressure (Hem et al., 1973); hence a metastable aluminosilicate is more likely to form. Paces (1978), calculated the disequilibrium index for an extensive set of natural and synthetic samples, and concluded that a reversible metastable aluminosilicate controls the Si and Al in natural waters. Hem et al. (1973), in laboratory experiments using synthetic solutions, found that halloysite ($Al_2Si_2O_5(OH)_4$) is precipitated. Halloysite is sometimes observed in shale, but mostly observed in volcanic and hydrothermal regions (Joussein et al., 2005 and references therein); halloysite has not been found at Rivendell. Fig. 10d shows that the concentration of dissolved Si decreases as pH increases; we thus hypothesize that the precipitation of metastable aluminosilicate determines Si in high cation concentration waters.

4.3. The chemistry evolution of the groundwater in Rivendell

The high-frequency time-series of W1 illustrates the dynamics of groundwater chemistry that could not have been captured by weekly or monthly sampling frequency. Unlike other wells, W1 is rarely diluted by recharge from rainstorms (Fig. 2). After the dilution events, W1 returns to high concentrations within several days after the cessation of the rainstorm (Fig. 9). For example, during a series of two large rainstorms (a) March 11 2011–April 1 2011 (total rain 460 mm; Fig. 9a) and (b) November 15–December 25 2012 (total rain 777 mm; Fig. 9b), all cations in W1 were diluted and then return high concentrations within days.

Two important aspects of W1's chemistry are keys to understanding the chemical evolution as water moves

downslope: first, the nearly constant chemistry at W1 even though its water table was highly responsive to the rainfall inputs; and second, the rapid dilution of W1 chemistry for some rainstorms when the water table was high. The first aspect may be explained by three competing hypotheses: (H1) rapid diffusion of cations from tightly bound and chemically mature water in the bedrock at W1; (H2) higher weathering rates in the W1 area; (H3) chemical evolution of low concentration water from the upslope to W1.

Diffusion of the bedrock water with high solute might be able to maintain the steady-state chemistry of W1. If true, however, the volume of the matrix water must be much greater than the mobile water. Otherwise, the solute concentrations in W1 would progressively decrease as the rainy season progresses; but W1 did not display a decreasing trend. We do not have porosity measurements at these wells to estimate the quantity of the matrix water; but since W1 is highly conductive (Fig. 6a), a large volume of water likely passes through W1. Therefore, H1 can be ruled out.

At W1, the water table is closer to the ground surface (−3 to −5 m) than at other wells and is also within the maximum rooting depth of vegetation (4 m; Canadell et al., 1996); hence significant effects of biological activity and supply of organic acids would be expected to enhance mineral dissolution rates (e.g. Banfield et al., 1999; Hamer et al., 2003). If enhanced biologically-driven weathering controls the chemistry of W1, element concentrations in the weathered bedrock forming the seasonally saturated zone at W1 would be more depleted than at W3 and W10; however, we did not find evidence to support this explanation. For example, weathering processes remove calcite first particularly in hydrologically active systems (White et al., 1999), like Rivendell. If W1 is more weathered than W3 and W10, calcite would be expected to be depleted in W1 relatively to W3 and W10; however, at W1, we found slightly higher calcite contents in core samples and even found calcite encrusting our pressure transducer, suggesting inflowing water already has high solute concentrations. Therefore, H2 can be ruled out.

For hypothesis 3, we note that the high frequency data show that all solutes were diluted and returned to high concentration values on the identical time scales, despite substantial differences in source minerals' dissolution rates. For instance, calcite ($10^{-7.68}$ mol m^{-2} s^{-1}; Arvidson et al., 2003) dissolves several orders of magnitude faster than chlorite and feldspars (10^{-12} (laboratory experiments) -10^{-17} (field measurements) mol m^{-2} s^{-1}; Jin et al., 2010; White and Brantley, 2003 reference therein). However, all solutes co-vary closely at W1, suggesting that chemical recovery is mainly due to the influx of high concentration water from upslope. But this high concentration chemistry at W1 throughout the rainy season, even when W3 and W10 displayed are dilute, suggests that W3 is unlikely to be the direct and primary source for W1. The source water of W1 may originate from upslope possibly via sandstone outcrop (Fig 1a; sandstone blocks dominate at W1) or via flows through deeper and isolated flow paths. These observations strongly imply that the groundwater is not a well-mixed reservoir; the water chemistry evolution will be governed by the material properties and flow paths. Although further study, such as a tracer experiment, is needed to identify the source of W1 water, H3 is most consistent with our observations.

Dilution events rarely occurred at W1, indicating that low concentration water is only transiently transported to W1 from upslope paths. These conductive paths may be via W3. Fig. 11a shows the concentration of Mg at W1 (colored symbols) as a function water table at W3 (vertical axis) and the total rainfall of the driving storms (horizontal axis and labeled points). This figure shows that Mg in W1, which represents all major cations' behavior, is diluted only when the W3 water level was high. Storms delivering as much as 104 mm of rainfall did not cause the dilution. Fig. 11b shows two corresponding properties of the weathered bedrock zone at W3. The open circles show the blow counts (number of drop counts, using a 140 pound (63.5 kg) weight dropped for 30-inch (760 mm), to penetrate a measured distance into the rock)) with a core barrel into the 5.1 cm diameter hole. The blow counts to −6 m were relatively low, suggesting mechanically weaker bedrock associated with open fractures and weathering. Visible signs of weathering persist to about −11 m and correspondingly blow counts rapidly climb to 50 counts/inch at −11 m and 400 counts/inch at about -14 m. The solid squares record the time it took for the water table to recover from the drawdown caused by the ISCO water sampling at W3

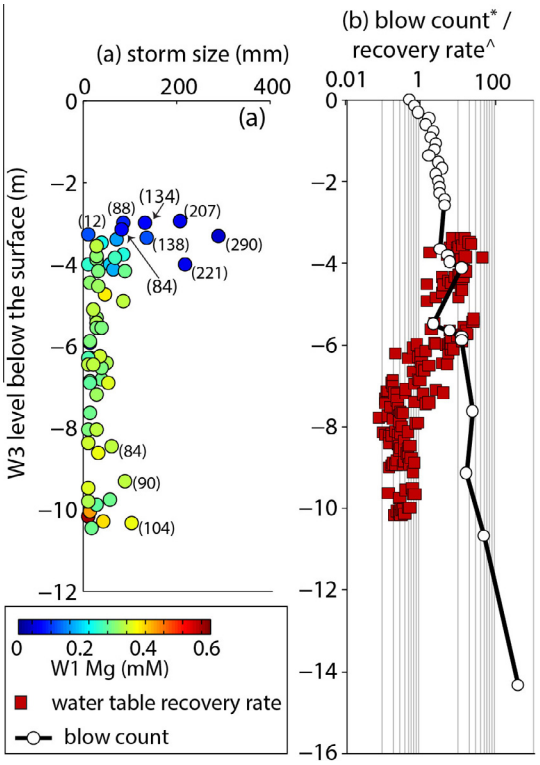

Fig. 11. (a) The minimum Mg in W1 during storm events and corresponding maximum W3 water-level. Numbers in parenthesis show the total amount of rain (mm) of storms; (b) Water table recharging rate (sample volume /recovery time) after the high-frequency water sampling (red square) and blow counts (open circle) of W3. * counts/inch; ^ L/day.

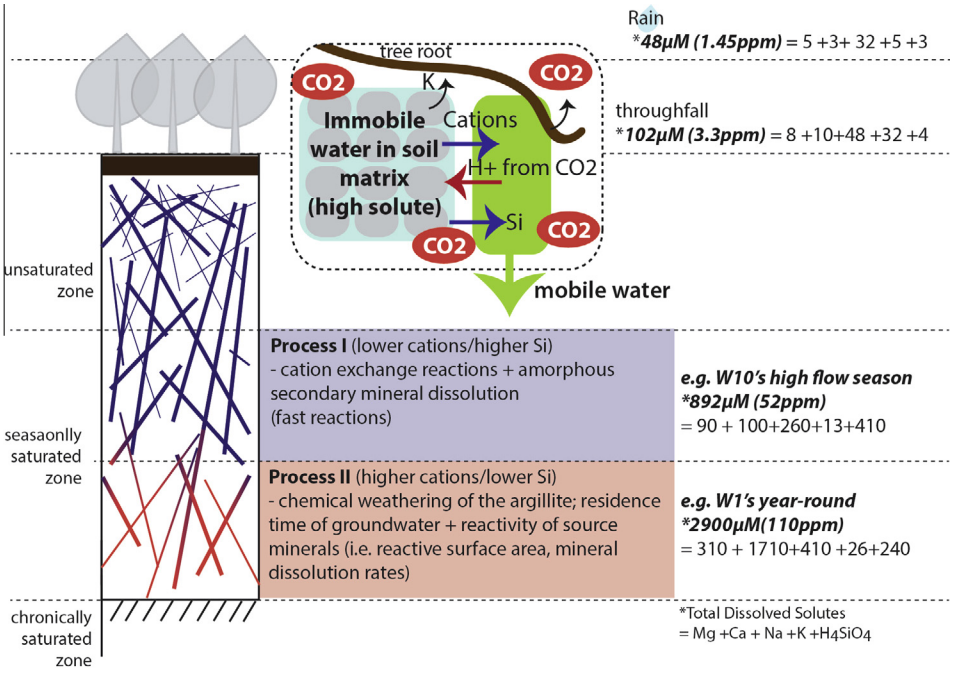

Fig. 12. Conceptual model for the chemical dynamics of bedrock groundwater in Rivendell. All infiltrated rainwater gains cations by cation exchange reactions and Si by dissolution of amorphous silica as passing through the unsaturated zone. This water may run through the highly conductive zone in the shallow seasonally saturated zone, and exit the hillslope within days to months. The recharged water in upslope also becomes concentrated as moving through the deeper seasonally saturated zone and its solute concentration is govern by thermodynamic equilibrium with reactive minerals.

(depth differences between before and after the sampling (cm) × cross section area of the well (=15.75 cm^2). This trend suggests that, above −6 m, where the blow counts decrease, the recovery rate was far faster, indicating the saturated conductivity rapidly increases. When W3 is at its shallowest depth, where the conductivity is greatest and presumably where the groundwater flows most rapidly, the concentrations at W1 is lowest and is similar to W3. Hence, we suggest that during high runoff events, the diluted water like that at W3 passes through W1.

In summary, we propose a conceptual model to explain the chemical dynamics of Rivendell groundwater (Fig. 12). First, infiltrated rainwater undergoes rapid pCO_2 enhanced cation exchange reactions and dissolution of amorphous Si while passing through the unsaturated zone. These waters increases its solute concentration by mineral dissolution/precipitation reactions with the argillite in the deeper weathered bedrock zone, evolving to higher concentrations that are set by equilibrium with primary and secondary minerals in the bedrock. Local differences, as recorded by the different temporal concentration dynamics at W1, may arise from different water flow paths and source bedrock. Our observations suggest that Rivendell's groundwater is not a well-mixed single reservoir even on the small scale of the studied drainage; however, we have defined that two dominant processes determining runoff chemistry.

In the Elder Creek catchment, overland flow has not been observed, except on the roads, and Salve et al. (2012) reported that all runoff occurred through the weathered bedrock zone. Because all rainwater infiltrates into the subsurface to drain to the stream, and cation exchange reactions are intense and rapid, we propose that the minimum concentrations of cations in the stream will be set the low concentrations developed during high flow conditions. During summer baseflow to Elder Creek, concentrations would be expected to rise, reflecting the high concentrations found at low water table.

4.4. Implications for chemical weathering modeling

Chemical weathering plays an important role in landscape evolution. Numerous studies on the weathering profile development have focused on what has remained in the hillslopes after chemical weathering while this study has focused on what departs the deep weathered zone under a hillslope. These two approaches study chemical weathering processes on substantially different time scales (hundreds of thousands or millions of years vs. individual storms to seasons), but together they provide complementary insight. Recently, Brantley et al. (2013) proposed that recharging of O_2- and CO_2-rich water to a deeper depth initiates pyrite oxidation and carbonate mineral dissolution, opening up porosity, causing the weathering front to propagate. We observe that, every year, W10 is recharged with new water, which has high O_2 and CO_2. At W10, calcite is depleted in the seasonally saturated zone compared with in the chronically saturated zone (Table 1). In addition, W1's groundwater is saturated with calcite year round, except for the dilution events. By combining these two approaches, our understanding on the development of the weathering front will be significantly improved.

5. CONCLUSION

High-frequency (1–3 days) observations of the hydrochemical dynamics of a groundwater system, which is perched on fresh bedrock and flows through a weathered bedrock zone, have been carried out from 2009 to 2012. This study has specifically focused on the temporal and spatial variability of Ca, Mg, Na, K and Si. The co-variation of water levels and solute concentration found at the mid- and upper slope wells suggest a shifting dominance of controlling processes. Cation concentrations decreased considerably as the water table rises in the mid to upslope areas, but the Si concentrations reach highest levels. We suggest that rainwater increases its cation concentration by proton driven cation exchange reactions enhanced by elevated subsurface pCO_2 and its Si concentration by dissolution of amorphous Si as it passes through the vadose zone. These concentrations are lowest at times of greatest runoff to the adjacent creek. Because all rainwater passes through the soil and unsaturated zone and the cation exchange reactions are rapid, possibly reaching equilibrium states within hours, we propose this process sets the minimum cation concentrations in the adjacent creek. Every year, this rainwater recharges the mid- and upslope wells (W3 and W10), and cation concentrations progressively increase during the summer groundwater recession season with the progression of weathering reactions. We propose that the high concentrations arise because of these waters reaching thermodynamic equilibrium with reactive minerals such as calcite (Ca), and clay minerals (i.e. Fe-rich chlorite (Mg), montmorillonite (K) and metastable aluminosilicate (Si)). Nonetheless, these waters are far from equilibrium with respect to primary minerals, for instance albite (Na). The lowest well, W1, shows little temporal variation of solute concentrations throughout the year except with rare dilution events occurring during high storm runoff. The W1 water must originate from upslope, but for much of the year, it does not seem to be derived from water found in the midslope area around W3, suggesting heterogeneous groundwater concentrations, perhaps associated with lithologic or deeper flow path variations.

Our direct, high-frequency observations reveal where (or how deep) in the weathered bedrock zone water flows, and specific processes and factors that are responsible for its chemistry: Controlling processes for the groundwater chemistry shift from rapid, vadose zone cation exchange reactions in the nearer surface to mineral equilibrium reactions at depth and slower runoff. Our study thus lays the groundwork for further exploration of both the spatial evolution of groundwater runoff and the coupled hydrologic and water chemistry dynamics within the critical zone that controls stream chemistry and eventually landscape evolution. Furthermore, our findings provide critical baseline information needed to evaluate the effect of extreme weather such as severe drought or extremely intense storms on the groundwater and stream chemistry.

ACKNOWLEDGEMENTS

We would like to thank two anonymous reviewers for providing insightful comments. This study was funded by the W.M. Keck Foundation (Berkeley HydroWatch Center Award), the National Science Foundation award (NSF-OCE1049222), the Department of Energy (DE-SC000147), and NSF CZP EAR - 1331940 for the Eel River Critical Zone Observatory. We are also grateful to the University of California Natural Reserve System for establishing the Angelo Coast Range Reserve as a protected site for our research. Todd Wood (LBNL) automated the remote sampling system and provided critical help with ICP-MS analyses. The Center for Environmental Biotechnology at Lawrence Berkeley National Laboratory generously offered their facilities for our soil/rock analysis. Daniella Rempe provided helpful discussion. UC Berkeley Undergraduate Research Apprenticeship Program interns Michael Fong, Nolan Wong, Tim Ault, Ernesto Martinez, Robert Nicklas, and Kevin Ni assisted both in the field and in the laboratory.

APPENDIX A. SUPPLEMENTARY DATA

Supplementary data associated with this article can be found, in the online version, at http://dx.doi.org/10.1016/j.gca.2014.05.011.

REFERENCES

Amacher M., Henderson R., Breithaupt M., Seale C. and Labauve J. (1990) Unbuffered and buffered salt methods for exchangeable cations and effective cation-exchange capacity. *Soil Sci. Soc. Am. J.* **54**, 1036–1042.

Anderson S. P., Dietrich W. E., Torres R., Montgomery D. and Loague K. (1997a) Concentration-discharge relationships in runoff from a steep unchanneled catchment. *Water Resour. Res.* **33**, 211–225.

Anderson S. P., Dietrich W. E., Montgomery D. R., Torres R., Conrad M. E. and Loague K. (1997b) Subsurface flow paths in a steep unchanneled catchment. *Water Resour. Res.* **33**(12), 2637–2653.

Anderson S. P. and Dietrich W. E. (2001) Chemical weathering and runoff chemistry in a steep headwater catchment. *Hydrol. Process.* **15**, 1791–1815.

Anderson S. P., von Blanckenburg F. and White A. F. (2007) Physical and chemical controls on the critical zone. *Elements* **3**, 315–319.

Appelo C. A. J. and Postma D. (2005) Ch. 6 ion exchange. In *Geochemistry Groundwater and Pollution*. Taylor & Francis, New York, pp. 241–309, second ed.

Arvidson R. S., Ertan I. E., Amonette J. E. and Luttge A. (2003) Variation in calcite dissolution rates: a fundamental problem?. *Geochim. Cosmochim. Acta* **67**(9) 1623–1634.

Asano Y., Uchida T. and Ohte N. (2003) Hydrologic and geochemical influences on the dissolved silica concentration in natural water in a steep headwater catchment. *Geochim. Cosmochim. Acta* **67**(11), 1973–1989.

Banfield J., Barker W., Welch S. and Taunton A. (1999) Biological impact on mineral dissolution: application of the lichen model to understanding mineral weathering in the rhizosphere. *Proc. Natl. Acad. Sci. USA* **96**, 3404–3411.

Banks E., Simmons C., Love A., Cranswick R., Werner A., Bestland E., Wood M. and Wilson T. (2009) Fractured bedrock and saprolit hydrogeologic controls on groundwater/surface-water interaction: a conceptual model (Australia). *Hydrogeol. J.* **17**, 1969–1989.

Brantley S. L., Holleran M. E., Jin L. and Bazilevskaya E. (2013) Probing deep weathering in the Shale Hills Critical Zone Observatory, Pennsylvania (USA): the hypothesis of nested

chemical reaction fronts in the subsurface. *Earth Surf. Process. Landforms* **38**(11), 1280–1298.

Calmels D., Galy A., Hovius N., Bickle M., West A. J., Chen M. and Chapman H. (2011) Contribution of deep groundwater to the weathering budget in a rapidly eroding mountain belt, Taiwan. *Earth Planet. Sci. Lett.* **303**, 48–58.

Campbell D. H., Clow D. W., Ingersoll G. P., Mast M. A., Spahr N. E. and Turk J. T. (1995) Processes controlling the chemistry of two snowmelt-dominated streams in the Rocky Mountains. *Water Resour. Res.* **31**(11), 2811–2821.

Canadell J., Jackson R. B., Ehleringer J. R., Mooney H. A., Sala O. E. and Schulze E. D. (1996) Maximum rooting depth of vegetation types at the global scale. *Oecologia* **108**, 583–593.

Cerling T., Pederson B. and Vondamm K. (1989) Sodium-calcium ion-exchange in the weathering of shales-implications for global weathering budgets. *Geology* **17**, 552–554.

Ciesielski H. and Sterckeman T. (1997) A comparison between three methods for the determination of cation exchange capacity and exchangeable cations in soils. *Agronomie* **17**, 9–16.

Clow D. W. and Drever J. I. (1996) Weathering rates as a function of flow through an alpine soil. *Chem. Geol.* **132**, 131–141.

Cosby B., Wright R., Hornberger G. and Galloway J. (1985) Modeling the effects of acid deposition – estimation of long-term water-quality responses in a small forested catchment. *Water Resour. Res.* **21**, 1591–1601.

Essington M. E. (2004) Chemical weathering. In *Soil and Water Chemistry: An Integrative Approach*. CRC Press, Boca Raton, pp. 101–127.

Faure G. (1998) Mineral stability diagrams. In *Principles and Applications of Geochemistry: A Comprehensive Textbook for Geology Students*. Prentice Hall, pp. 172–199, second ed.

Fuller T., Perg L., Willenbring J. and Lepper K. (2009) Field evidence for climate-driven changes in sediment supply leading to strath terrace formation. *Geology* **37**, 467–470.

Garrels R. M. (1984) Montmorillonite/illite stability diagrams. *Clay. Clay Mineral.* **32**(3), 161–166.

Gibs J., Brown G. A., Turner K. S., MacLeod C. L., Kelinski J. C. and Koehnlein S. A. (1993) Effects of small-scale vertical variations in well-screen inflow rates and concentrations of organic compounds on the collection of representative groundwater-quality samples. *Ground Water* **31**(2), 201–208.

Hamer M., Graham R., Amrheim C. and Bozhilov K. (2003) Dissolution of ripidolite (Mg, Fe-chlorite) in organic and inorganic acid solutions. *Soil Sci. Soc. Am. J.* **67**, 654–661.

Haria A. H. and Shand P. (2004) Evidence for deep sub-surface flow routing in forested upland Wales: implications for contaminant transport and stream flow generation. *Hydrol. Earth Syst. Sci.* **8**(3), 334–344.

Hem. J. D., Roberson C. E., Lind C. J. and Polzer W. L. (1973) Chemical interactions of aluminum with aqueous silica at 25C°. In *Geochemical Survey Water-Supply Paper: 1827-E*, U. S. Govern. Print. Off., Washington.

Holloway J. M. and Dahlgren R. A. (2001) Seasonal and event-scale variations in solute chemistry for four Sierra Nevada catchments. *J. Hydrol.* **250**, 106–121.

International Atomic Energy Agency and United Nations Educational Scientific and Cultural Organization (2001) Chemistry of carbonic acid in water. In *Environmental isotopes in the hydrological cycle: Principles and applications Vol.1 (*eds. W.G. Mook). Available from: <http://www-naweb.iaea.org/napc/ih/IHS_resources_publication_hydroCycle_en.html>.

Jin L., Andrews D., Holmes G., Lin H. and Brantley S. L. (2011) Opening the "Black Box": water chemistry reveals hydrological controls on weathering in the susquehanna shale hills critical zone observatory. *Vadose Zone J.* **10**, 928–942.

Jin L., Ravella R., Ketchum B., Bierman P., Heaney P., White T. and Brantley S. L. (2010) Mineral weathering and elemental transport during hillslope evolution at the Susquehanna/Shale Hills Critical Zone Observatory. *Geochim. Cosmochim. Acta* **74**, 3669–3691.

Joussein E., Petit S., Churchman J., Theng B., Righi D. and Delvaux B. (2005) Halloysite clay minerals – a review. *Clay Mineral.* **40**, 383–426.

Kennedy V. C. (1971) Silica variation in stream water with time and discharge. In *Nonequilibrium system in natural water chemistry* (ed. J. Hem). Advanced in Chemistry, American Chemical Society, Washington, DC, pp. 94–130.

Kenoyer G. J. and Bowser C. J. (1992) Groundwater chemical evolution in a sandy silicate aquifer in northern Wisconsin:1 Patterns and rates of change. *Water Resour. Res.* **28**(2), 579–589.

Kim H., Bishop J., Wood T. and Fung I. (2012) Autonomous water sampling for long-term monitoring of trace metals in remote environments. *Environ. Sci. Technol.* **46**, 11220–11226.

Kittrick J. (1982) Solubility of 2 high-Mg and 2 high Fe chlorites using multiple equilibra. *Clays Clay Miner.* **30**, 167–179.

Lock J., Kelsey H., Furlong K. and Woolace A. (2006) Late Neogene and Quaternary landscape evolution of the northern California Coast Ranges: evidence for Mendocino triple junction tectonics. *Geol. Soc. Am. Bull.* **118**(9–10), 1232–1246. http://dx.doi.org/10.1130/B25885.1.

Legout C., Molenat J., Aquilina L., Gascuel-Odoux C., Faucheux M., Fauvel Y. and Bariac T. (2007) Solute transfer in the unsaturated zone-groundwater continuum of a headwater catchment. *J. Hydrol.* **332**, 427–441.

Martin-Hayden J. M. (2000) Controlled laboratory investigations of wellbore concentration response to pumping. *Ground Water* **38**(1), 121–128.

McLaughlin R. J., Ellen S., Blake, Jr., M., Jayko A. S., Irwin W., Aalto K., Carver G. and Clake, Jr., S. (2000) Geology of the Cape Mendocino Eureka Garberville and southwestern part of the Hayfork 30×60 min quadrangles and adjacent offshore area northern California. *U.S. Geol. Surv. Misc. Field Stud. MF 2336*.

Montgomery D., Dietrich W. E., Torres R., Anderson S. P., Heffner J. and Loague K. (1997) Hydrologic response of a steep unchanneled valley to natural and applied rainfall. *Water Resour. Res.* **33**, 91–109.

Mulholland P. J., Wilson G. V. and Jardine P. M. (1990) Hydrogeochemical response of a forested watershed to storms: effects of preferential flow along shallow and deep pathways. *Water Resour. Res.* **26**(12), 3021–3036.

Oh N. and Richter D. (2004) Soil acidification induced by elevated atmospheric CO_2. *Glob. Change Biol.* **10**, 1936–1946.

Paces M. (1978) Reversible control of aqueous aluminum and silica during the irreversible evolution of natural waters. *Geochim. Cosmochim. Acta* **42**, 1487–1493.

Rice K. C. and Bricker O. P. (1995) Seasonal cycles of dissolved constituents in stream water in two forested catchments in the mid-Atlantic region of the eastern USA. *J. Hydrol.* **170**, 137–158.

Rouxel M., Molenat J., Ruiz L., Legout C., Faucheux M. and Gascuel-Odoux G. (2011) Seasonal and spatial variation in groundwater quality along the hillslope of an agricultural research catchment (Western France). *Hydrol. Process.* **25**, 831–841.

Soulsby C., Chen M., Ferrier R. C., Helliwell R. C., Jenkins A. and Harriman R. (1998) Hydrogeochemistry of shallow groundwater in an upland Scottish catchment. *Hydrol. Process.* **12**, 1111–1127.

Salve R., Rempe D. and Dietrich W. E. (2012) Rain rock moisture dynamics and the rapid response of perched groundwater in weathered fractured argillite underlying a steep hillslope. *Water Resour. Res.* **48**, W11528.

Shand P., Haria A. H., Neal C., Griffiths K. J., Goody D. C., Dixon A. J., Hill T., Buckley D. K. and Cunningham J. E. (2005) Hydrochemical heterogeneity in an upland catchment: further characterization of the spatial temporal and depth variations in soils streams and groundwaters of the Plynlimon forested catchment Wales. *Hydrol. Earth Syst. Sci.* **9**(6), 621–644.

Shand P., Farbyshire F. D. P., Gooddy D. and Haria A. H. (2007) $^{87}Sr/^{86}Sr$ as an indicator of flowpaths and weathering rates in the Plynlimon experimental catchments Wales UK. *Chem. Geol.* **236**, 247–265.

Sollins P., Grier C., McCorison F., Cromack K. and Fogel R. (1980) The internal element cycles of an old-growth Doulas-fir ecosystem in Western Oregon. *Ecol. Monogr.* **50**, 261–285.

Sposito G. (2008) *The chemistry of soils*, second ed. Oxford University Press Oxford, New York.

Tournassat C., Gailhanou H., Crouzet C., Braibant G., Gautier A. and Gaucher E. (2009) Cation exchange selectivity coefficient values on smectite and mixed-kayer illite/smectite minerals. *Soil Sci. Soc. Am. J.* **73**, 928–942.

Tromp-van Meerveld H., Peters N. and McDonnell J. (2007) Effect of bedrock permeability on subsurface stormflow and the water balance of a trenched hillslope at the Panola Mountain Research Watershed Georgia USA. *Hydrol. Process.* **21**, 750–769.

Uchida T., Asano Y., Ohte N. and Mizuyama T. (2003) Seepage area and rate of bedrock groundwater discharge at a granitic unhandled hillslope. *Water Resour. Res.* **39**(1), 1018.

United States Department of Agriculture (2009) Soil survey filed and laboratory methods manual; S*oil survey investigations report No. 51 Version 1.0* (edt Rebecca Burt) National Soil Survey Center National Resources Conservation Service, U.S. Department of Agriculture Lincoln, Nebraska.

United States Environmental Protection Agency (1996) Method 1669: Sampling ambient water for trace metals at EPA water quality criteria levels; United State Environmental Protection Agency Office of Water Engineering and Analysis Division: Washington DC.

Van der Hoven S., Solomon D. and Moline G. (2005) Natural spatial and temporal variations in groundwater chemistry in fractured sedimentary rocks: scale and implications for solute transport. *Appl. Geochem.* **20**, 861–873.

Wang Q., Yuncong Li. and Klassen W. (2005) Determination of cation exchange capacity on low to highly calcareous soils. *Commun. Soil Sci. Plan.* **36**, 1479–1498.

White A. F., Bullen T. D., Vivit D. V., Schulz M. S. and Clow D. W. (1999) The role of disseminated calcite in the chemical weathering of granitoid rocks. *Geochim. Cosmochim. Acta* **63**(13/14), 1939–1953.

White A. F. and Brantley S. L. (2003) The effect of time on the weathering of silicate minerals: why do weathering rates differ in the laboratory and field? *Chem. Geol.* **202**, 479–506.

Williams M. W., Brown A. D. and Melack J. M. (1993) Geochemical and hydrologic controls on the composition of surface water in a high-elevation basin, Sierra Nevada, California. *Limnol. Oceanogr.* **38**(4), 774–797.

Wilson C. J. and Dietrich W. E. (1987) The contribution of bedrock groundwater flow to storm runoff and high pore pressure development in hollows. Erosion and Sedimentation in the Pacific Rim (Proceedings of the Corvallis Symposium August) *IAHS Publ. No. 165*.

Yeghicheyan D., Carignan J., Valladon M., Bouhnik Le Coz M., Le Cornec F., Castrec-Rouelle M., Robert M., Aquilina L., Aubry E., Churlaud C., Dia A., Deberdt S., Dupre B., Freydier R., Gruau G., Henin O., de Kersabiec A., Mace J., Marin L., Morin N., Petitjean P. and Serrat E. (2001) A compilation of silicon and thirty one trace elements measured in the natural river water reference material SLRS-4(NRC-CNRC). *Geostandard Newslett.* **25**(2–3), 465–474.

Associate editor: Marc Norman